Large-Scale Fabrication of Boron Nitride Nanosheets and Their Utilization in Polymeric Composites with Improved Thermal and Mechanical Properties

By *Chunyi Zhi,* Yoshio Bando, Chengchun Tang, Hiroaki Kuwahara,* and *Dimitri Golberg*

Recent progress in understanding 2D ordered crystals of graphene.[1] has attracted more and more researchers to the nanosheet field. Undoubtedly, physics, chemistry, and applications of 2D materials are quite rich.[2–4] For example, the relativistic nature of charge carriers in graphene may lead to breakthroughs in future electronic devices.[5–8] Moreover, graphene has obvious advantages compared to carbon nanotubes (CNTs) when used in polymeric composites.[9,10] These studies have triggered new interests in 2D-ordered crystals of elements other than carbon, such as transition-metal dichalcogenides, perovskites, etc.[11–14]

Boron nitride (BN) is a structural analog of carbon. Similar to graphite, diamond, and CNT phases, BN has layered (hexagonal, *h*-BN), cubic, and tubular structures. BN has comprehensive applications due to many unmatched properties. For example, *h*-BN is frequently used as a solid lubricant in rigorous environments, as an ultraviolet-light emitter,[15–19] or as an insulating thermoconductive filler in composites.[20,21] It is believed that a 2D ordered BN crystal structure with an exposed (002) crystal surface would be valuable to exploit many unique properties of a graphitic-like (002) plane, such as superb high thermal conductivity, mechanical strength, and others. In addition, a BN nanosheet (BNNS) is a unique insulating 2D system to explore. It is noted that Pacilé et al.[22] first reported on the synthesis of 2D BN nanostructures and Han et al.[23] fabricated double- and monolayered BN sheets. However, the product yields were scarce due to limitations of fabrication methods adopted. Therefore, the detailed studies on microstructures and applications of BNNSs have not been yet performed.

Here, we report on the large-scale fabrication of 2D BNNSs and the production of their polymeric composites. Detailed morphological and structural microscopic studies were carried out and detailed property investigations of the new composite materials were performed. Polymeric composites containing BNNSs exhibited a remarkable reduction of the coefficient of thermal expansion (CTE) and possessed enhanced elastic modulus and strength.

Vigorous sonication was able to exfoliate BNNSs from the precursor BN particles. A strong polar solvent, *N,N*-dimethylformamide (DMF), was used. Prior to the work, we expected that the strong interactions between the polar DMF molecules and a BN surface would facilitate exfoliation, similar to graphite exfoliation.[24] Also, we suggested that the solvents could be optimized by choosing a proper media whose surface energy matches the energy per unit area required to overcome the van der Waals forces while peeling BN nanoparticles away. It was also noted that, different from BN nanotubes synthesized by a chemical vapor deposition (CVD) method, the BNNSs could be easily redispersed in various organic solvents, such as chloroform, DMF, and others. This indicates that their surfaces are in a quite different chemical status. However, we found difficult to accurately study the surface functional groups by means of Fourier transform infrared spectroscopy, because of the low signal intensities and overlapped peaks reflecting the –OH, –NH, and –BN bonds (see Supporting Information). Detailed studies using other alternative techniques are under way.

Figure 1 shows a scanning electron microscopy (SEM) image of a pristine BN powder and BNNSs obtained using the

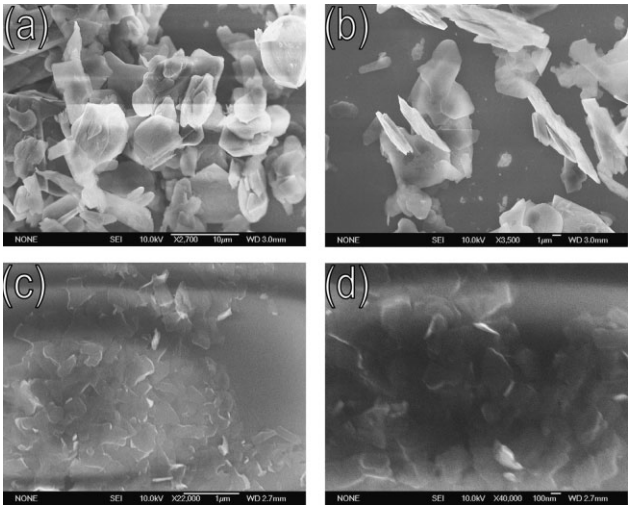

Figure 1. a,b) SEM images of BN nanoparticles used as precursors for the BNNSs fabrication. c,d), SEM images of 2D BNNSs; optical contrast is weak because of very thin flakes and their insulating electrical properties.

[*] Dr. C. Y. Zhi, Prof. Y. Bando, Prof. C. C. Tang, Prof. D. Golberg
World Premier International Center for Materials Nanoarchitectonics (MANA)
National Institute for Materials Science
Namiki1-1, Tsukuba, Ibaraki 305-004 (Japan)
E-mail: zhi.chunyi@nims.go.jp
Dr. H. Kuwahara
Innovation Research Institute, Teijin Ltd.,
2-1, Hinode-cho, Iwakuni
Yamaguchi 740-8511 (Japan)

DOI: 10.1002/adma.200900323

sonication–centrifugation process. The sonication is able to peel off BNNSs from the particles due to interactions between solvent molecules and particle surfaces. As shown in Figure 1c and d, the BNNSs have micrometer dimensions. Their thicknesses cannot be accurately deduced from the SEM images. Notably, not only the BN particle thicknesses are reduced, but also the lateral sizes of the (002) BNNSs flakes become smaller, compared to pristine particles. This implies that sonication can peel off a BNNS from some defective areas of precursor BN particles.

Transmission electron microscopy (TEM) was used to further analyze the BNNSs structures. Due to ultimately thin shapes, the BNNSs were entirely transparent to an electron beam, as shown in Figure 2a and b, the low-magnification TEM images of the sheets. Figure 2c and d shows a high- resolution TEM image and its enlarged view. The incident electron beam was along the [002] direction, thus perpendicular to the (002) crystal face. It is well known that *h*-BN is isostructural to graphite, except for the different stacking sequences of atomic planes. Highly crystallized graphite possesses a Bernal (AB) stacking sequence, while *h*-BN is stacked with the B atoms above and beneath the corresponding N atoms. If the discrepancy between B and N atoms is not considered, *h*-BN has the AAA... stacking order. It should be noted that the alternating white and black dots shown in Figure 2c and d do not directly correspond to the real images of the B and N atoms.[25] The distances between each two neighboring white dots in Figure 2c is actually equal to the distances between any two nearest N or B atoms. They are equal to the (100) lattice constant too. In the inset to Figure 2c, the TEM contrast-intensity profiles recorded along the marked red line reveals that the fringe separation is ~0.25 nm. According to the geometrical relationship, inset to Figure 2d, the spacing between B and N atoms is deduced to be ~1.43 Å, which is quite close to the well-known length of a B–N bond of 1.44 Å. Figure 2e and f show a TEM image and electron-diffraction pattern of a BNNS. The pattern reveals a typical six-fold symmetry natural of *h*-BN. It should be noted that according to calculations the intensity of dots of {1100} and {2110} should be very similar (see Supporting information), thus it is concluded that the variation of intensity is due to structural non-uniformity of the BNNSs. This can be the rolling topography of the surface or the thickness variation.

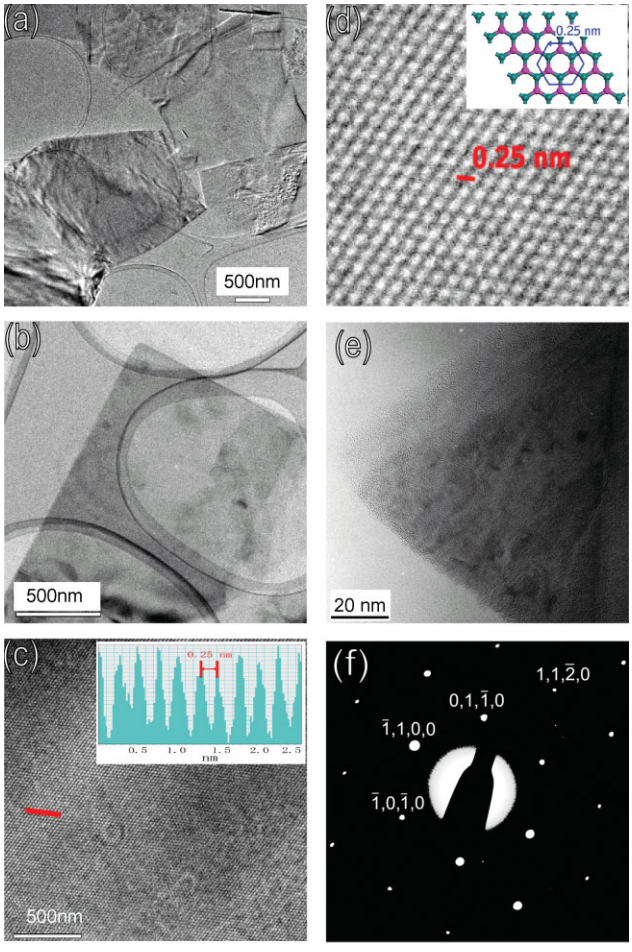

Figure 2. a,b) Low-magnification TEM images of BNNSs. c,d) High-resolution TEM images of BNNSs at different magnifications: the incident electron beam is perpendicular to the (002) face. Inset to c) TEM contrast intensity profile recorded along the marked red line reveals that the fringe separation is ~0.25 nm. Inset to d) Structure model of BNNSs. e,f) TEM image and corresponding electron-diffraction pattern revealing typical six-fold symmetry.

Accidentally, some BNNSs have curled edges, rendering it possible to evaluate a sheet thickness during TEM, as shown in Figure 3. The average thickness of a BNNS was dependent on centrifugation speed. At 5000 rpm, most of the sheets have less than 20 layers, that is, the thickness is less than 7 nm, whereas at 8000 rpm the thickness is reduced to 3 nm (less than 10 layers). Statistics of the sheet thicknesses after 5000 rpm centrifugation is shown in Figure 3d. There were 52 BNNSs with a thickness less than 7 nm over a total 73 nanosheets studied. The thinnest BNNSs observed were three-layered, as illustrated in Figure 3c. From these images, the lattice distance is deduced to be ~0.35 nm, quite close to the (002) interplanar distance in a standard layered BN.

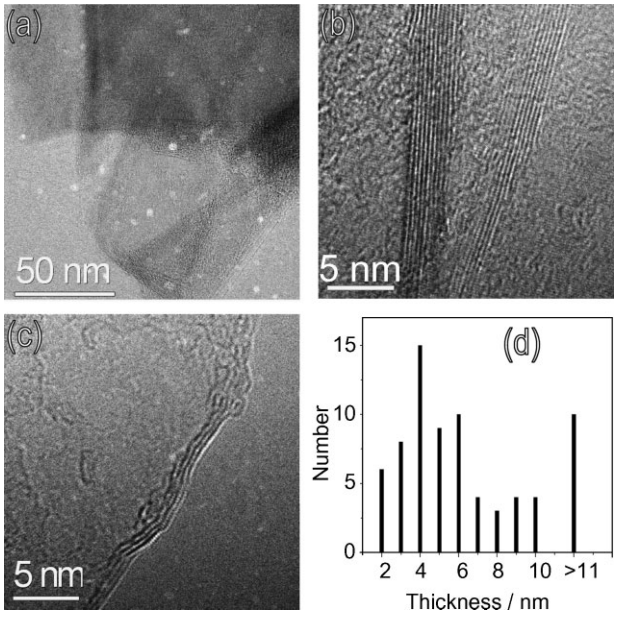

Figure 3. a) TEM image showing BNNSs with curled edges. b,c) TEM images displaying BNNSs with a thickness of around 4 nm, 3 nm, and 1.2 nm. d) Statistics of BNNSs' thickness distribution.

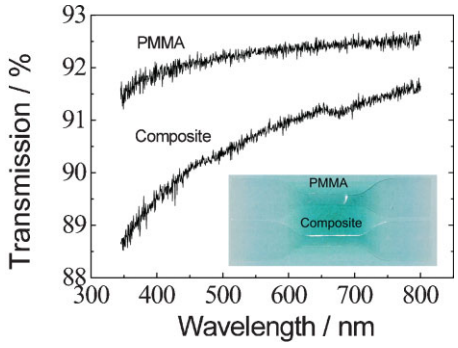

Figure 4. Comparative optical transparency tests on blank PMMA (upper curve) and its BNNS composite (lower curve). The inset shows the composite films cut in slices for tensile tests.

Compared to other 2D materials, BNNSs can ultimately display all the advantages of the (002) crystal faces of a graphitic-like structure, such as high mechanical strength, elasticity, high thermal conductivity. Thus, they should be able to significantly improve the related properties of a polymer matrix. Therefore, using the present milligram BNNSs quantities, we fabricated novel Polymethyl methacrylate (PMMA)/BNNSs composites and analyzed their properties.

The composite films obtained had almost the same transparency as the blank PMMA films. The difference could not be identified with a naked eye, as shown in the inset to Figure 4. A UV–vis absorption apparatus was used to analyze the films in more detail. PMMA, which is typically used as an organic glass, possesses high transparency along all wavelengths, up to around 92% transmission. After embedding BNNSs, the transmission of light at a wavelength longer than 600 nm is quite close to that of the blank PMMA, up to 91%. Only when the wavelength becomes shorter than 600 nm, the transmission of the composite compared to the blank PMMA starts to diminish. Nevertheless, roughly, the transmission of the composite is kept up to 90% along the whole range of wavelengths. The reason for the regarded fast decline in composite transmission in the violet range might be due to BN fillers, which are wide-band-gap materials, and thus have stronger absorption within the violet- and ultraviolet-light ranges.

Thermal mechanical analysis (TMA) was then carried out, and the coefficients of thermal expansion (CTE) of the blank PMMA and the composite films were compared (Fig. 5a). Apparently, the embedment of BNNSs effectively reduces the CTE of PMMA. Prior to the glass-transition temperature, the CTE was reduced from 184 to 160 ppm $^{\circ}C^{-1}$, whereas after the glass transition, the efficiency was even more striking, with the CTE reduced from 28 200 to 13 000 ppm $^{\circ}C^{-1}$. It should be particularly emphasized that such remarkable changes are documented for very low BNNS fractions in PMMA, only 0.3 wt%. This indicates that BNNSs effectively restrict the mobility of polymer chains.[26]

Moreover, embedment of BNNSs in PMMA results in mechanical reinforcement, as shown in Figure 5b and c. It is noted that for blank PMMA (prepared using DMF as a solvent) the elastic modulus was slightly lower than when chloroform was used as solvent, which is consistent with our previous observations.[27,28] After embedment of BNNSs, the elastic modulus of PMMA increased from 1.74 to 2.13 GPa (22% increase), and the strength also increased (11% increase). This indicates that an applied mechanical load can effectively be transferred to BNNSs due to profound interfacial interactions. For comparison, in our recent experiments, BN nanotubes were used to reinforce PMMA, and at a 1 wt% BN nanotube fraction, a 19% improvement of the elastic modulus was achieved, but the strength slightly decreased due to an increase in defect concentration associated with BN nanotube embedment.[28] This indicates that BNNSs are able to interact with the polymer chains more effectively. Besides, our results rival the cases for other advanced fillers. For example, in the Lee's experiments with CNTs, the tensile strength of a CNTs/PMMA nanocomposite

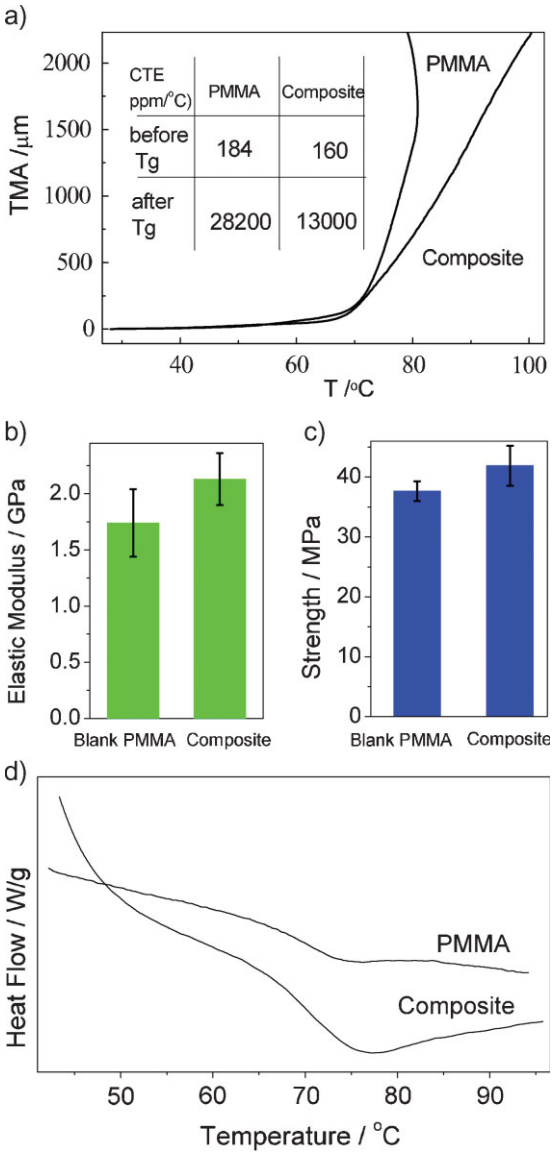

Figure 5. a) Comparative TMA tests on blank PMMA and its BNNS composite. 5 mm long square-like samples were used for tests. The inset shows the CTE data before and after the glass-transition temperature deduced from the measured TMA curves. b,c) Summaries of measured elastic modulus and strength of blank PMMA and its BNNS composites. d) DSC curves of PMMA and its BNNS composites. The T_g of PMMA and the composites are 69.7 and 72.0°C, respectively.

increased by ~15% and the tensile toughness increased by ~17.5% (for a 1 wt% CNT fraction) with respect to blank PMMA.[29,30]

The present improvements in CTE and tensile properties are attributed to three factors. First, due to very-thin morphologies, the distortions induced by exfoliation may result in wrinkled sheet topologies. Such nanoscale surface roughness may enhance mechanical interlocking with polymer chains.[31] The second factor is that, different from the highly symmetrical C–C bonds, the B–N bonds possess ionic characteristics, which may induce a polarized surface suitable for interacting with a polar polymer, such as PMMA used in the experiments. Third, as mentioned above, perfect dispersion of BNNSs in many organic solvents indicates that there might be some organic functional groups on their surfaces. These may also promote the interfacial interactions between PMMA and BNNSs. The direct evidence of enhanced interactions is a variation in glass-transition temperature (T_g), shown in Figure 5d, and the shapes of differential scanning calorimetry (DSC) curves for PMMA and its BNNS composites. T_g is estimated from the midpoint of a heat-capacity peak, which is slightly shifted from 69.7 to 72.0°C. This indicates that the mobility of polymer chains is affected due to confinement and strength of polymer–surface interactions. The chains that are in contact with BNNSs would exhibit slower dynamics than those within a polymer matrix. This, in turn, leads to an increase in the configuration entropy and an increase in T_g.

In summary, we report an efficient method to fabricate high-yield 2D BNNSs using a sonication–centrifugation technique. This method has the following advantages: i) milligram levels of BNNSs are achievable; ii) ultimately pure BNNSs are obtained based on a highly pure precursor; iii) average nanosheet thickness is adjusted by the centrifugation speed. The nanosheets have micrometer dimensions in plane, whereas their thicknesses can be as small as ~1.2 nm (only three atomic BN layers). The microstructures of the sheets were characterized in detail using TEM and SEM. Finally, PMMA/BNNSs transparent composites were fabricated. The CTE for the composite films were remarkably reduced,and the glass-transition temperature was also affected compared to blank polymers. This indicates that the polymer-chain mobility decreases due to efficient matrix interactions with the embedded BNNSs. A 22% improvement in the elastic modulus of PMMA and an 11% increase in its strength were obtained with only 0.3 wt% BNNSs fraction utilized.

This study paves the way for novel fundamental and application studies of BNNSs. The nanosheets should find applications in optoelectronic devices, composite optical windows, and heat-releasing materials. Compared with previously studied BN nanotubes, whose 100% pure CVD production in a few-walled morphology is difficult, preparation of the BNNSs is easily scalable, and thus more technological. In addition, their specific 2D structures lead to better dispersibility in polymers improving the resultant composite performance.

Experimental

BNNSs were prepared through exfoliation of *h*-BN microsized particles. In a typical experimental run, BN powder (1 g, Aldrich, used as received) in DMF (40 mL) was tip-type sonicated to disperse the powder for 10 h. The solution was then centrifuged at 5000–8000 rpm in order to remove residual large-size BN particles. The solution was dropped on a TEM grid or silicon wafers for the SEM and TEM analyses, or dried to obtain pure BNNSs. Around 0.5–1 mg BNNSs could be routinely obtained from 1 g BN powder as a precursor and after 10 h sonication.

A solution method was used to fabricate the composites, as reported elsewhere [28].

A scanning electron microscope (JEOL SM67F) was used to characterize BNNSs. TMA was carried out on a TMA-60 analyzer (Shimadzu Corporation, Japan). The microstructures were analyzed using a JEOL-3000F high-resolution field-emission transmission electron microscope operated at 300 kV. The UV–vis absorption experiments were performed using a HITACHI U-4100 spectrometer. Tensile tests were carried out using a EZ-S-100N machine made by Shimadzu Corporation. For DSC measurements, an SII Exstar6000 DSC6220 apparatus (Seiko Instruments, Inc., Tokyo, Japan) was utilized. The curves were recorded for the second heating cycle with a heating speed of 5 °C min^{-1}. Supporting Information is available online from Wiley InterScience or from the author.

Received: January 29, 2009
Revised: February 15, 2009
Published online: April 14, 2009

[1] K. S. Novoselov, A. K. Geim, S. V. Morosov, D. Jiang, Y. Zhang, S. V. Dubonos, I. V. Grigorieva, A. A. Firsov, *Science* **2004**, *306*, 666.
[2] D. Li, M. B. Müller, S. Gilje, R. B. Kaner, G. G. Wallace, *Nat. Nanotechnol.* **2008**, *3*, 101.
[3] K. S. Novoselov, A. K. Geim, S. V. Morozov, D. Jiang, M. I. Katsnelson, I. V. Grigorieva, S. V. Dubonos, A. A. Firsov, *Nature* **2005**, *438*, 197.
[4] M. I. Katsnelson, K. S. Novoselov, A. K. Geim, *Nat. Phys.* **2006**, *2*, 620.
[5] Y. B. Zhang, Y.-W. Tan, H. L. Stormer, P. Kim, *Nature* **2005**, *438*, 201.
[6] S. Y. Zhou, G.-H. Gweon, A. V. Fedorov, P. N. First, W. A. de Heer, D.-H. Lee, F. Guinea, A. H. Castro Neto, A. Lanzara, *Nat. Mater.* **2007**, *6*, 770.
[7] T. Ohta, A. Bostwick, T. Seyller, K. Horn, E. Rotenberg, *Science* **2006**, *313*, 951.
[8] A. Bostwick, T. Ohta, T. Seyller, K. Horn, E. Rotenberg, *Nat. Phys.* **2007**, *3*, 36.
[9] S. Stankovich, D. A. Dikin, G. H. B. Dommett, K. M. Kohlhass, E. J. Zimney, E. A. Stach, R. D. Piner, S. T. Nguyen, R. S. Ruoff, *Nature* **2006**, *442*, 282.
[10] T. Ramanathan, A. A. Abdala, S. Stankovich, D. A. Dikin, M. Herrera-Alonso, R. D. Piner, D. H. Adamson, H. C. Schniepp, X. Chen, R. S. Ruoff, S. T. Nguyen, I. A. Aksay, R. K. Prudhomme, L. C. Brinson, *Nat. Nanotechnol.* **2008**, *3*, 327.
[11] J. C. Meyer, A. K. Geim, M. I. Katsnelson, K. S. Novoselov, T. J. Booth, S. Roth, *Nature* **2007**, *446*, 60.
[12] J. S. Bunch, A. M. van der Zande, S. S. Verbridge, I. W. Frank, D. M. Tanenbaum, J. M. Parpia, H. G. Craighead, P. L. McEuen, *Science* **2007**, *315*, 490.
[13] J. C. Meyer, A. K. Geim, M. I. Katsnelson, K. S. Novoselov, D. Obergfell, S. Roth, C. Girit, A. Zettl, *Solid State Commun.* **2007**, *143*, 101.
[14] K. S. Novoselov, D. Jiang, F. Schedin, T. J. Booth, V. V. Khotkevich, S. V. Morozov, A. K. Geim, *Proc. Natl. Acad. Sci.* **2005**, *102*, 10451.
[15] E. Hernández, C. Goze, P. Bernier, A. Rubio, *Phys. Rev. Lett.* **1998**, *80*, 4502.
[16] A. P. Suryavanshi, M. Yu, J. Wen, C. Tang, Y. Bando, *Appl. Phys. Lett.* **2004**, *84*, 2527.
[17] P. Kim, L. Shi, A. Majumdar, P. L. McEuen, *Phys. Rev. Lett.* **2001**, *87*, 215502.
[18] X. Blasé, A. Rubio, S. G. Louie, M. L. Cohen, *Europhys. Lett.* **1994**, *28*, 335.
[19] K. Watanabe, T. Taniguchi, H. Kanda, *Nat. Mater.* **2004**, *3*, 404.
[20] G. Lee, M. Park, J. Kim, J. I. Lee, H. G. Yoon, *Composties: Part A* **2006**, *37*, 727.

[21] G. Pezzotti, I. Kamada, S. J. Miki, *Eur. Ceram. Soc.* **2000**, *20*, 1197.
[22] D. Pacilé, J. C. Meyer, Ç. Girit, A. Zettl, *Appl. Phys. Lett.* **2008**, *92*, 133107.
[23] W. Q. Han, L. J. Wu, Y. M. Zhu, K. Watanabe, T. Takiguchi, *Appl. Phys. Lett.* **2008**, *93*, 223103.
[24] Y. Hernandez, V. Nicolosi, M. Lotya, F. M. Blighe, Z. Sun, S. De, I. T. Mcgovern, B. Holland, M. Byrne, Y. K. Gun'ko, J. J. Boland, P. Niraj, G. Duesberg, S. Krishnamurthy, R. Goodhue, J. Hutchison, V. Scardaci, A. C. Ferrari, J. N. Coleman, *Nat. Nanotechnol.* **2008**, *3*, 563.
[25] D. Golberg, Y. Bando, L. Bourgeois, K. Kurashima, T. Sato, *Appl. Phys. Lett.* **2000**, *77*, 1979.
[26] G. Lee, M. Park, J. Kim, J. I. Lee, H. G. Yoon, *Composties: Part A* **2006**, *37*, 727.
[27] C. Y. Zhi, Y. Bando, C. Tang, S. Honda, H. Kuwahara, *J. Mater. Res.* **2006**, *21*, 794.
[28] C. Y. Zhi, W. L. Wang, Y. Bando, C. Tang, H. Kuwahara, *J. Nanomater.* **2009**, **2008**, *2008*, article ID 624036 .
[29] W. J. Lee, S. E. Lee, C. G. Kim, *Compos. Struct.* **2006**, *76*, 406.
[30] L. Q. Liu, H. D. Wagner, *Compos. Interface.* **2007**, *14*, 285.
[31] G. D. Smith, D. Bedrov, L. W. Li, O. J. Byutner, *Chem. Phys.* **2002**, *117*, 9478.